Prog. Theor. Phys. Vol. 126, No. 3, September 2011, Letters

Gamma-Ray Burst without Baryonic and Magnetic Load?

Kunihito Ioka, Yutaka Ohira, Norita Kawanaka and Akira Mizuta

KEK Theory Center and Graduate University for Advanced Studies (Sokendai), Tsukuba 305-0801, Japan

(Received March 29, 2011; Revised August 4, 2011)

We show that, contrary to common belief, internal shocks can arise in an accelerating radiation-dominated jet if it is confined even weakly to a converging opening angle because the acceleration declines. The radiation-dominated internal shock (RDIS) enables a very efficient yet highly nonthermal emission by Fermi-like photon acceleration, keeping the electron-positron ($e^{\pm}$) pair photosphere and inertia up to a high Lorentz factor > 1000. In gamma-ray bursts (GRBs), a weak confinement would persist beyond the progenitor star or surrounding matter because of the fast cocoon accompanying the breakout jet. The simplest model predicts few high-energy cosmic rays and neutrinos, and a correlation between the early afterglow and the GeV-TeV prompt emission. The central engine allows a less fine-tuned baryon load than previously thought, even including pure-leptonic unmagnetized outflows.

Subject Index: 410, 413, 416, 480, 484

GRB and baryon load Gamma-Ray Bursts (GRBs) are the most luminous objects in the universe. It remains a big challenge to reveal how most of the energy can be converted into gamma rays with highly nonthermal spectra.[1),2)]

The baryon load is a key parameter for the fireball dynamics and emission. The original fireball model[3),4)] was pure leptonic with the photon-to-baryon ratio $\eta \equiv L/\dot{M}c^2 = \infty$. As the fireball expands, the $e^{\pm}$ pairs annihilate and almost all the energy is released to thermal radiation: it is efficient but inconsistent with nonthermal observations. This leads to the baryon-loaded model with $\eta \lesssim 10^3$, in which the radiation energy is converted to the kinetic energy of matter,[5)] and then back to the radiation by internal shocks within variable outflows.[6)–8)] By its very nature, however, this standard picture faces an efficiency problem.[9),10)] The Lorentz factor dispersion required for the efficient reconversion is too large to reproduce the observed spectral correlations $\nu_{\rm peak} \propto L^{1/2}$.[11)–13)] This brings forth the photosphere model[14)–19)] that invokes a partial thermalization near the photosphere to stabilize the peak energy $\nu_{\rm peak}$ at the thermal peak, while retaining the nonthermal spectrum. The observed Band spectrum could be reproduced by Comptonization of the thermal photons via dissipation such as shocks[19)–21)] and magnetic reconnections.[14),22)]

These matter-dominated models assume the baryon load in the range (see Fig. 1)

$$10^2 \lesssim \eta \left(\equiv \frac{L}{\dot{M}c^2}\right) \lesssim 10^3, \tag{1}$$

to avoid the compactness problem[1)] (for $10^2 \lesssim \eta$) and the predominant thermal emission[23)] (for $\eta \lesssim 10^3$), where the baryon-poor fireball with $\eta \gtrsim 10^3$ is considered to emit thermal photons because no internal shocks occur in the radiation-dominated

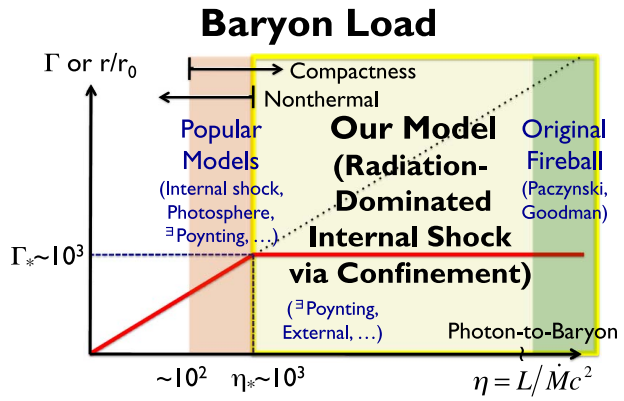

Fig. 1. We categorize GRB models on the basis of the baryon load. Popular models usually assume the photon-to-baryon ratio $\eta = L/\dot{M}c^2$ from $10^2 \lesssim \eta$ (to avoid the compactness problem) to $\eta \lesssim 10^3$. We consider the radiation-dominated jet with $\eta \gtrsim 10^3$, including the pure-leptonic original fireball model.[3),4)] Such jets were considered to cause no internal shocks before being transparent at the Lorentz factor $\Gamma \sim 10^3$ and radius $r/r_0 \sim 10^3$, and hence, emit (dominant) thermal radiation unlike in observations.[23)] This picture is changed by the jet confinement.

fireball, which accelerates as $\Gamma \propto r$ with the preceding shell always faster than the succeeding one. Therefore, the inferred baryon load is only limited within one order of magnitude, in contrast to a huge variety of GRBs. We may identify it as the "*fine-tuning problem of the baryon load*". Although the baryon-rich fireballs could be just unobservable with selection bias, there seems no compelling reason to believe $\eta \lesssim 10^3$. Recent Fermi observations[24)–26)] have made the problem even worse[19)] by detecting high-energy photons to limit the Lorentz factor $\Gamma \gtrsim 10^3$, i.e., $\eta \gtrsim 10^3$ in some bursts (despite the controversies on the numerical factor[27)–29)]).

One possible solution to the fine-tuned baryon load problem is the Poynting-dominated model.[14),22),30)–33)] Even without (electrons associated with) baryon, the energy is released only nonthermally via magnetic reconnections. Many uncertainties still remain, especially in the dissipation site. It may also be difficult to keep the jet cold in the hot photon pool near the central engine.

The other possibility may be the externally induced dissipation by the oblique shocks[34)–36)] or the entrainment of baryon[19)] during the acceleration. However, the external dissipation only occurs at the causally connected periphery of the jet, and the strong confinement ($\theta < \Gamma^{-1}$) is necessary for the full dissipation across the jet.

In this paper, we show that, contrary to popular belief, the radiation-dominated jet can cause internal shocks if the geometry is confined even weakly (even $\theta > \Gamma^{-1}$) by some external pressure or internal magnetic field. This could markedly expand the available parameter space to $10^3 \lesssim \eta$ as outlined below.

Two shell model We envisage that the Lorentz factor Γ of an outflow fluctuates by a factor of $\Delta\Gamma \sim$ a few around its mean. This may be modeled by two shells ejected from a radius r_0 at times t_1 and $t_2 = t_1 + \Delta t$ (where $\Delta t > 0$) with different initial Lorentz factors Γ_1 and $\Gamma_2 (> \Gamma_1)$, respectively (allowing for the possibility of $\Gamma_i \gg 1$ as in the jets breaking out of the progenitor star). The shell trajectory is

given by

$$\frac{dr}{dt} = c\beta = c\sqrt{1 - \frac{1}{\Gamma^2}}. \tag{2}$$

For the conical (or spherical) radiation-dominated jet $\Gamma \propto r$, we can easily integrate Eq. (2) as $r = \{(r_0^2/\Gamma_i^2) + [c(t - t_i) + r_0\beta_i]^2\}^{1/2}$, $(i = 1, 2)$. Two shells collide at

$$\frac{r}{r_0} = \frac{1}{\mathcal{R}}\left[1 + \left(\frac{1}{2\Gamma_1^2} + \frac{1}{2\Gamma_2^2}\right)\mathcal{R}^2 + \left(\frac{1}{4\Gamma_1^2} - \frac{1}{4\Gamma_2^2}\right)^2 \mathcal{R}^4\right]^{1/2}, \tag{3}$$

if the following condition is satisfied,

$$\mathcal{R} \equiv \frac{2}{\beta_2^2 - \beta_1^2}\left(\beta_2 - \beta_1 - \frac{c\Delta t}{r_0}\right) > 0. \tag{4}$$

If the interval Δt exceeds a critical time, $c\Delta t > (\beta_2 - \beta_1)r_0$, i.e., $\mathcal{R} < 0$, even a photon cannot catch up with the accelerating fore shell (see Fig. 2).

The catch-up condition (4) is not usually fulfilled by the physical processes because the radial velocity dispersion spreads the shell width before the start $r < r_0$ and the next shell is delayed by the causal time, $\Delta t \gtrsim r_0/c\beta_1$ for the non-relativistic case and $\Delta t \gtrsim r_0/2c\Gamma_1^2$ [and, hence, $\mathcal{R} \lesssim -\Gamma_1^2/(\Gamma_2^2 - \Gamma_1^2)$] for the relativistic case, leading to no collision. This is the essential reason why we have not considered the internal shock in the radiation-dominated jet, although a short timescale may be produced by a small-scale magnetic reconnection or a jet opening angle of less than $\sim 1/\Gamma^2$.

However, the Lorentz factor evolves differently from the conical one $\Gamma \propto r$ to

$$\Gamma \propto \left(\frac{r}{r_0}\right)^{\lambda}, \tag{5}$$

if the jet is confined to a converging opening angle,

$$\theta \propto r^{\lambda - 1}, \quad (\lambda < 1) \tag{6}$$

by some external pressure or internal magnetic field. This is because the comoving volume evolves differently from the conical one[1)] to $V' \sim \pi\theta^2 r^2 \Gamma\Delta \propto r^{2\lambda}\Gamma$, where the lab-frame width Δ remains constant if it is smaller than the spreading width $\sim r/\Gamma^2$. The adiabatic expansion of radiation (with an adiabatic index $\gamma_a = 4/3$) decreases the comoving temperature as $T' \propto V^{1-\gamma_a} \propto V'^{-1/3} \propto r^{-2\lambda/3}\Gamma^{-1/3}$. A solid boundary conserves the total energy $\Gamma T'^4 V' \propto \Gamma T' = \text{const}$, which yields Eq. (5).

For the confined jet $\lambda < 1$, the catch-up condition differs from Eq. (4). We can analytically integrate the trajectory in Eq. (2) considering (hereafter) the relativistic case $\Gamma_2 > \Gamma_1 \gg 1$ with an expansion $\beta \simeq 1 - \Gamma^{-2}/2$. Then, the shells collide at

$$\frac{r}{r_0} \simeq \left[1 - \frac{c\Delta t}{\frac{1}{2\lambda - 1}\left(1 - \frac{\Gamma_1^2}{\Gamma_2^2}\right)\frac{r_0}{2\Gamma_1^2}}\right]^{\frac{1}{1-2\lambda}} \equiv \mathcal{R}_\lambda^{\frac{1}{1-2\lambda}}, \quad \text{if } \mathcal{R}_\lambda > 0. \tag{7}$$

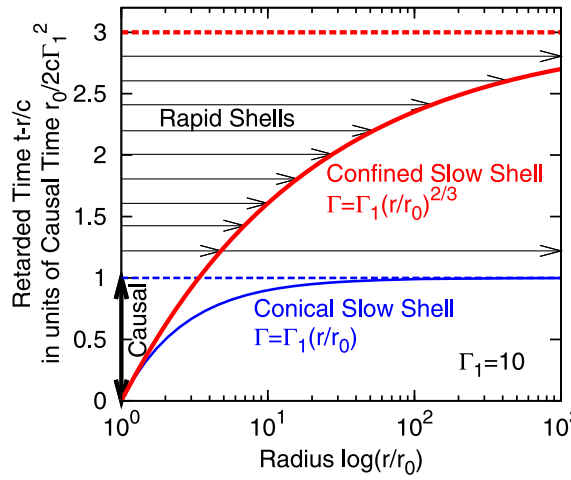

Fig. 2. A spacetime diagram for the retarded time $t - r/c$ in units of the causal time $r_0/2c\Gamma_1^2$ as a function of the radius $\log(r/r_0)$, using $\Gamma \gg 1$. A photon travels horizontally in this diagram. A conical radiation-dominated jet $\Gamma \propto r$ (solid line) approaches a light path, so that any rapid jet emitted after the causal time $\sim r_0/2c\Gamma_1^2$ cannot catch up with it. Meanwhile, a confined jet accelerates more slowly $\Gamma \propto r^\lambda$ (thick solid line) in a converging opening angle $\theta \propto r^{\lambda-1}$ with $\lambda < 1$, enabling internal shocks with rapid jets (arrows) over a wide radius range.

Note that $\mathcal{R}_\lambda = \mathcal{R}$ for $\lambda = 1$ and $\Gamma_2 > \Gamma_1 \gg 1$ in Eqs. (4) and (7).

The qualitative properties change at $\lambda = 1/2$.

(i) *Strong confinement case*, $\lambda \le 1/2$: The collision always occurs ($\mathcal{R}_\lambda > 0$) for any interval Δt, simply because the causal region $\sim r/2\Gamma^2 \propto r^{1-2\lambda}$ monotonically increases in the lab frame. This is almost the same as the usual internal shock after the acceleration ceases.[7),8)] Meanwhile, since $\theta < \Gamma^{-1}$, the jet boundary is also causally connected with the jet axis. This enables the recollimation or oblique shocks across the jet. Therefore, the jet can be dissipative during the expansion with shocks in the causal region. Note that the strong confinement ($\theta\Gamma < 1$) is employed to accelerate the Poynting-dominated jet to the matter-dominated jet.[32),33)]

(ii) *Weak confinement case*, $1/2 < \lambda < 1$: The catch-up condition $\mathcal{R}_\lambda > 0$ in Eq. (7) requires that the interval Δt is less than a critical time $\Delta t_{\rm crit}$,

$$c\Delta t < \frac{1}{2\lambda - 1}\left(1 - \frac{\Gamma_1^2}{\Gamma_2^2}\right)\frac{r_0}{2\Gamma_1^2} \equiv c\Delta t_{\rm crit}. \tag{8}$$

This can be satisfied by the causal processes (i.e., with the next shell ejected after the causal time $\Delta t \gtrsim r_0/2c\Gamma_1^2$), in contrast to the conical jet ($\lambda = 1$), because the prefactor $(2\lambda-1)^{-1}(1-\Gamma_1^2/\Gamma_2^2)$ can be larger than unity due to the slow acceleration $\Gamma \propto r^\lambda$. The space-time diagram in Fig. 2 is useful to understand the following.

(A) The radiation-dominated jet can cause internal shocks even during the acceleration if the jet is more collimated than the conical shape, $\lambda < 1$ in Eq. (5).

(B) The shock can occur at a large radius since an accelerating shell asymptotically approaches a light path (see dashed lines in Fig. 2). The shock radius is large

when the interval Δt gets close to the critical time $\Delta t_{\rm crit}$ where the time-fraction vanishes $\mathcal{R}_\lambda = 1 - \Delta t/\Delta t_{\rm crit} = 0$ in Eqs. (7) and (8).

(C) The slow shell can be repeatedly shocked by the successive rapid shells, which can be ejected with shorter intervals $\sim r_0/2c\Gamma_2^2$ than the slow shells $\sim r_0/2c\Gamma_1^2$.

In the weak confinement, the causality is lost across the jet ($\theta\Gamma > 1$). Although the angular structure of Γ would arise depending on the initial condition, the acceleration is likely reduced because of denser streamlines (smaller V') than in the conical case. If the confinement is strong initially (inside the star) and weak later (outside the star), the oblique shock does not necessarily accompany the weak confinement phase.

Jet confinement by cocoon The jet would be confined by the progenitor star (long GRB) or the surrounding dense matter or wind[37] (short GRB).[36),38)–40)] Note that the merger of two neutron stars ejects baryons before the collapse to a black hole even with an ordinary magnetic field strength.[37)] As the jet runs into the stellar envelope, the shocked jet and envelope flow sideways (if $\theta < \Gamma_h^{-1}$) and inflate a cocoon, whose pressure confines the jet. We can roughly estimate the index λ in Eqs. (5) and (6) by considering the pressure balance at

(I) the jet head: The longitudinal balance of the ram pressure between the jet $\sim L_j/\pi\theta^2 r^2 c$ and the stellar matter $\sim \rho_* c^2 \beta_h^2$ determines the jet head velocity $c\beta_h \sim c(L_j/\pi c^3 \rho_* r^2)^{1/2}\theta^{-1}$.

(II) the cocoon-envelope boundary: The cocoon expands with a speed $c\beta_c$ by balancing the ram pressure of the ambient matter $\sim \rho_* c^2 \beta_c^2$ and the cocoon pressure $\sim L_j t/(c\beta_h t)(c\beta_c t)^2$ which is the total energy deposited by the jet divided by the volume of the cocoon, so that $\beta_c \sim (L_j/c^3\rho_* r^2)^{1/4}\beta_h^{1/4} \sim (L_j/c^3\rho_* r^2)^{3/8}\theta^{-1/4}$ with $r \sim c\beta_h t$.

(III) the jet-cocoon boundary: The cocoon pressure $\sim \rho_* c^2 \beta_c^2$ confines the radiation-dominated (hot) jet with the transverse pressure $p_j \sim L_j/\pi\theta^2 r^2 c\Gamma^2$, leading to $\theta \sim (L_j/c^3\rho_* r^2)^{1/6}\Gamma^{-4/3}$.

Substituting the envelope profile $\rho_* \sim r^{-n}$, $\Gamma \propto r^\lambda$ in Eq. (5), $\theta \propto r^{\lambda-1}$ in Eq. (6), and a constant luminosity $L_j \sim$ const, we can equate the radial dependence to find

$$\lambda \sim \frac{4+n}{14}. \quad \left(\theta \propto r^{(n-10)/14} \text{ inside the star } \rho_* \sim r^{-n}\right) \tag{9}$$

The ideal radiative envelope has an index $n = 3$ (i.e., $\lambda \sim 1/2$), whereas more realistic presupernova models such as 16TI[41)] have shallower slopes $n \sim 2$ (i.e., more confinement $\lambda \sim 3/7$). Because of the strong confinement $\lambda \leq 1/2$, the jet is basically dissipative before the jet breakout. Similar dissipation is observed in the simulations.[34),42),43)] The Lorentz factor of the jet at the breakout is around

$$\Gamma_b \sim \left(\frac{r_*}{r_{\rm ISCO}}\right)^\lambda \sim 10\text{–}30, \tag{10}$$

where $r_* \sim 10^{10}$ cm is the stellar radius (breakout radius) and $r_{\rm ISCO} \sim 10^7$ cm is the central engine size. The variability timescale is about $\sim r_*/c\Gamma_b^2$, which is $\sim r_{\rm ISCO}/c$ for $\lambda = 1/2$, so that the central engine timescale may be marginally preserved.

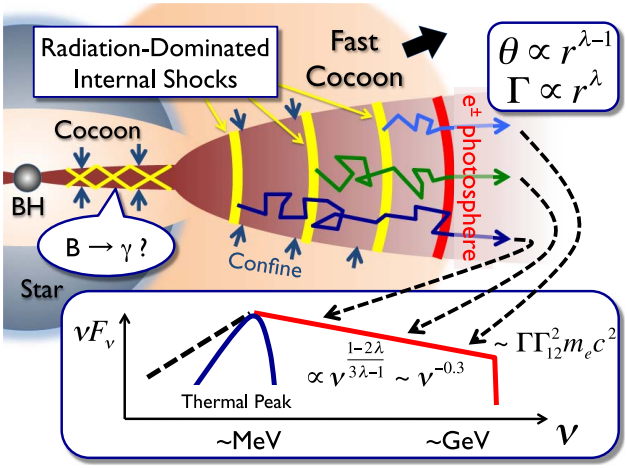

Fig. 3. Radiation-dominated internal shocks (RDISs) can occur if the jet is confined in $\theta \propto r^{\lambda-1}$ with $\lambda < 1$, for example, by the fast cocoon pressure [Eq. (11)], because the jet acceleration slows down $\Gamma \propto r^{\lambda}$ [Eq. (5)]. The RDISs accelerate photons and create $e^{\pm}$. The nonthermal photons are generated from extended radii, where lower energy photons originate deeper with more scatterings [Eqs. (15) and (16)] before emerging from the $e^{\pm}$ photosphere [Eq. (14)]. In this paper, we do not account for the low-energy spectral slope.

Even after the jet breakout, the jet would be confined to some extent. A plausible source of pressure is the fast cocoon that just escapes from the jet head sideways at the breakout. The fast cocoon is thereby fast (ranging from $\Gamma \sim 1$) up to the jet Lorentz factor at the breakout $\sim \Gamma_b$ in Eq. (10), and confines the following jet with a lag time δt over a long distance $\sim c\delta t\Gamma_b^2 \sim 10^{13}(\delta t/1\ \mathrm{s})(\Gamma_b/30)^2$ cm. Also, the transverse pressure of the fast cocoon is initially comparable to that of the jet p_j, and then declines slower $p_c \propto T'^4 \propto V'^{-4/3} \propto r^{-8/3}$ than $p_j \sim L_j/\pi\theta^2 r^2 c\Gamma^2 \propto r^{-4\lambda}$ if the jet were conical ($\lambda = 1$), because the fast cocoon becomes matter-dominated[*)] with the coasting expansion $V' \sim 4\pi r^2 \Gamma\Delta \propto r^2$. For $p_c \sim p_j$, the jet is confined,

$$\lambda \sim \frac{2}{3}. \quad (\theta \propto r^{-1/3} \text{ outside the star}) \tag{11}$$

The confinement gets weaker than inside the star (with index larger than the boundary $\lambda > 1/2$) but still continues (in the weak regime $1/2 < \lambda < 1$). Thus, the dissipation proceeds via the internal shocks caused by the variability due to the central engine or the jet-envelope interaction. The initial opening angle would be the inverse of the Lorentz factor $\theta_0 \sim \Gamma_b^{-1} \sim 0.03$–$0.1$ in Eq. (10) at the stellar surface $r_0 \sim r_* \sim 10^{10}$ cm, and the product $\Gamma\theta \propto r^{2\lambda-1}$ grows afterward, as required for the afterglow observations of jet breaks.

[*)] The fast cocoon may be initially radiation-dominated and expand to $\Gamma \sim \gamma'_p\Gamma_b \sim \Gamma_b^2$ after converting the radiation energy into the bulk motion, where $\gamma'_p \sim \Gamma_b$ is the random Lorentz factor per proton at the shock, as in the collisionless bulk acceleration.[19)] Then, the Lorentz factor of the fast cocoon may range from $\Gamma \sim 1$ to $\sim \Gamma_b^2$. This effect could alter λ in Eq. (11).

$e^{\pm}$ photosphere and high Γ with internal shocks When the rapid jet catches up with the slow one, an internal shock forms, which dissipates the relative kinetic energy. The relative Lorentz factor at the collision is the same as the initial value,

$$\Gamma_{12} \simeq \frac{1}{2}\left(\frac{\Gamma_2}{\Gamma_1} + \frac{\Gamma_1}{\Gamma_2}\right), \tag{12}$$

since $\Gamma \propto r^{\lambda}$ for both jets. For the radiation-dominated jet, the kinetic energy is almost carried by photons, which is transferred by Compton scatterings of $e^{\pm}$, forming a radiation-mediated shock.[44] A small fraction of photons are repeatedly upscattered across the shock, extending a power-law spectrum to high energies like the Fermi acceleration (Blandford-Payne mechanism).[45),46] Even for a moderate optical depth, $\tau_T \sim$ a few, the Compton y-parameter $y \sim \tau_T \beta_{12}^2 \Gamma_{12}^2$ can exceed unity for the relativistic shocks. After the shock passage, the turbulent motion induced by, for example, Richtmyer-Meshkov instability, also provides the scattering centers, continuing the photon acceleration.[14),47] Then, an appreciable fraction of the relative kinetic energy can go to high-energy photons and create $e^{\pm}$ pairs.

The $e^{\pm}$ pair creation can continue to a large radius since the collision radius rapidly grows as the jets expand owing to radiation pressure [see Eqs. (7) and (8) and Fig. 2]. The jet acceleration holds as long as the $e^{\pm}$ pairs trap the radiation. The maximum Lorentz factor is limited by the condition that the system becomes transparent $\tau_T \sim n'_{\pm}\sigma_T c t'_{\rm dyn} \sim 1$, where $n'_{\pm} = f_{\pm}L/4\pi r^2 m_e c^3 \Gamma^2$ is the comoving number density of $e^{\pm}$ pairs, $t'_{\rm dyn} \sim r/c\Gamma$ is the comoving dynamical time, L is the isotropic total luminosity and $f_{\pm}$ is the energy fraction of $e^{\pm}$ pairs. Then, the coasting Lorentz factor is

$$\Gamma_{\pm} = \left(\frac{\Gamma_0^{1/\lambda} f_{\pm} L \sigma_T}{4\pi m_e c^3 r_0}\right)^{\frac{\lambda}{3\lambda+1}} \simeq 2900 \left(\frac{\Gamma_0}{30}\right)^{1/3} \left(\frac{r_0}{10^{10}\ {\rm cm}}\right)^{-2/9} \left(\frac{f_{\pm}L}{10^{53}\ {\rm erg\ s^{-1}}}\right)^{2/9}, \tag{13}$$

at the $e^{\pm}$ photosphere of radius

$$r_{\pm} \sim r_0 \left(\frac{\Gamma_{\pm}}{\Gamma_0}\right)^{1/\lambda} \sim 1 \times 10^{13}\ {\rm cm}\ \left(\frac{\Gamma_0}{30}\right)^{-1} \left(\frac{r_0}{10^{10}\ {\rm cm}}\right)^{2/3} \left(\frac{f_{\pm}L}{10^{53}\ {\rm erg\ s^{-1}}}\right)^{1/3}, \tag{14}$$

where (and hereafter) we suppose a jet breaking out of the stellar surface, $r_0 \sim r_* \sim 10^{10}$ cm and $\Gamma_0 \sim \Gamma_b \sim$ 10–30 in Eq. (10), with $\lambda = 2/3$ in Eq. (11) in the last equalities. The pair energy fraction $f_{\pm}$ is about the energy fraction emitted above the pair creation threshold $\sim \Gamma_{\pm} m_e c^2 \sim$ GeV, and $f_{\pm} \sim 1$ is implied in Fermi bursts. The high Lorentz factor $\Gamma_{\pm} > 10^3$ is also consistent with the Fermi observations.

Nonthermal photospheric spectrum The radiation-dominated jet emits almost all the energy from the $e^{\pm}$ photosphere, which is nonthermalized by internal shocks. The spectrum would have a thermal peak with a high-energy power-law tail. We illustrate the spectral shaping using a constant-luminosity model: equal-energy rapid jets are ejected after a slow jet at intervals of the causal time $\Delta t_{\rm sh} \sim r_0/2c\Gamma_2^2$ ($\ll r_0/2c\Gamma_1^2$) (see Fig. 2). The internal shocks can repeat in the dynamical time of the slow jet

and create sufficient $e^{\pm}$ pairs to sustain the opacity. Thus, the $e^{\pm}$ pair density is mainly determined by the $e^{\pm}$ annihilation as $n'_{\pm} \sim 1/\sigma_T c \Delta t'_{\rm sh}$ after a time $\Delta t'_{\rm sh}$ following a shock. The interval of shocks is redshifted in the comoving frame as $\Delta t'_{\rm sh} \sim \Gamma \Delta t_{\rm sh} \sim \Gamma r_0/2c\Gamma_2^2$. Then, the typical optical depth of the jet evolves as

$$\tau_T \sim n'_{\pm}\sigma_T c t'_{\rm dyn} \sim \frac{t'_{\rm dyn}}{\Delta t'_{\rm sh}} \sim \frac{r/c\Gamma}{\Gamma r_0/2c\Gamma_2^2} \propto \frac{r}{\Gamma^2} \propto r^{1-2\lambda} \sim r^{-1/3}. \tag{15}$$

Note that $\tilde{\tau}_T \propto \tilde{n}'_{\pm} t'_{\rm dyn} \propto V'^{-1} r/\Gamma \propto r^{-4\lambda+1} \propto r^{-5/3}$ (steeper) if $e^{\pm}$ were conserved.

Under the photosphere $\tau_T > 1$, thermal photons carry the dominant energy at a (nonrelativistic) comoving temperature $h\nu'_{\rm peak} < m_e c^2$ with a number density $n'_{\rm peak} \sim f_{\pm}^{-1} n'_{\pm} m_e c^2/h\nu'_{\rm peak}$. In this cool bath, $e^{\pm}$ cools by $\Delta T'_e/T'_e \sim -h\nu'_{\rm peak}/m_e c^2$ in a single Compton scattering, and becomes thermal in a time less than the dynamical time, $t'_{{\rm cool},e} \sim (n'_{\rm peak}\sigma_T c)^{-1}|T'_e/\Delta T'_e| \sim t'_{\rm dyn} f_{\pm}/\tau_T < t'_{\rm dyn}$. The nonthermal photons with $\nu' > \nu'_{\rm peak}$ also lose energy $\Delta\nu'/\nu' \sim (4kT'_e - h\nu')/m_e c^2 \sim -h\nu'/m_e c^2$ in a single scattering by the cooled $e^{\pm}$. However, the cooling time exceeds the dynamical time, $t'_{{\rm cool},\gamma} \sim (n'_{\pm}\sigma_T c)^{-1}|\nu'/\Delta\nu'| > t'_{\rm dyn}$, at $h\nu' < m_e c^2/\tau_T$. Therefore, the spectrum remains nonthermal below the observed frequency $\sim \Gamma\nu'$ ($\sim$ const),

$$\nu \sim \frac{\Gamma m_e c^2}{h\tau_T} \propto r^{3\lambda-1} \sim r^1, \tag{16}$$

even if the photons are generated below the photosphere $r < r_{\pm}$ with $\tau_T > 1$. At $\tau_T > 1$, the photons are trapped since the diffusion time is $t_{\rm diff} \sim \tau_T^2/n'_{\pm}\sigma_T c \sim \tau_T t_{\rm dyn}$.

The internal shock extends the spectrum to a flat power law, injecting a fair fraction of the shock energy at the frequency in Eq. (16). In the constant-luminosity model, the injected shock energy is proportional to the number of shocks $\sim t'_{\rm dyn}/\Delta t'_{\rm sh}$, so that the emergent spectrum at the photosphere is

$$\nu F_\nu \propto \frac{t'_{\rm dyn}}{\Delta t'_{\rm sh}} \propto r^{1-2\lambda} \propto \nu^{(1-2\lambda)/(3\lambda-1)} \sim \nu^{-0.3}, \tag{17}$$

with Eqs. (15) and (16). Interestingly, this is consistent with the high-energy Band spectrum of GRBs $\nu F_\nu \propto \nu^{-0.3\pm0.3}$.[1),2)] The nonthermal photons are generated from radii extending over several orders, where the lower energy photons originate deeper below the photosphere with more scatterings in Eqs. (15) and (16).

Our model naturally explains the observations that the nonthermal energy above $\nu_{\rm peak}$ is comparable to the thermal energy because the radiation itself nonthermalizes the radiation. In the constant-luminosity model, the slow jets (mainly for thermal energy) and rapid jets (mainly for nonthermal energy) have comparable energies if they are ejected for a similar duration of the causal time of the slow jets $\sim r_0/2c\Gamma_1^2$ (see Fig. 2).

The rapid jets could become transparent via $e^{\pm}$ annihilation before colliding with the slow jet. The released photons expand conically and only a part of them $\sim (\theta/\theta_0)^2 \propto r^{2\lambda-2}$ could shock the slow jet. The loss of shocked energy softens the spectrum as $\nu F_\nu \propto r^{1-2\lambda} \times r^{2\lambda-2} \propto \nu^{1/(1-3\lambda)} \sim \nu^{-1}$ with Eqs. (16) and (17),

which is still consistent with the observations. The angular structure of λ [below Eq. (8)] could also cause diversity to the high-energy index. The released photons could be absorbed by the rear jets with different streamlines, or by the surrounding (optically thick) fast cocoon, possibly developing the hollow cone-structured jet with $\Gamma \sim \Gamma_b \sim 10$–$30$ for the shallow X-ray afterglow (see below). The decoupled $e^{\pm}$ from the rapid jet could be caught up with by other rear jets and create further $e^{\pm}$.

Implications

• *GeV-TeV spectrum and delay* – The photospheric spectrum may extend to $\nu_{\max} \sim \Gamma_{\pm}\Gamma_{12}^2 m_e c^2 \sim 10\ \mathrm{GeV}(\Gamma_{\pm}/3000)(\Gamma_{12}/3)^2$,[44] where we expect the $e^{\pm}$ creation cutoff and possibly the (blue-shifted and broadened) annihilation line,[16),17)] providing closure relations[48] for Fermi and CTA to verify the $e^{\pm}$ photosphere. We may also expect a spectral break at $\nu \sim \Gamma_{\pm}\Gamma_{12} m_e c^2$ due to the Klein-Nishina effect.

The GeV onset delay observed in Fermi bursts[24)–26)] may be explained by the leading jet that is not confined by the fast cocoon and, hence, cannot keep internal shocks and $e^{\pm}$ to a high Lorentz factor. In this picture, the delay time is about $\sim r_{\pm}/c\Gamma_b^2 \sim 1$ s in Eqs. (10) and (14), as observed.

The (collisionless) internal shocks continue beyond the photosphere within $e^{\pm}$ outflows after the radiation decoupling, and could produce the observed extra GeV component, possibly up to TeV, by synchrotron or inverse Compton emission.[19),49)] The luminosity can be appreciable up to $\sim f_{\pm}L$.

• *Early afterglow* – The prompt emission is radiatively efficient $1 - f_{\pm} \gtrsim 50\%$, and the remaining kinetic energy of $e^{\pm}$ powers the early afterglow. The $e^{\pm}$ energy fraction $f_{\pm}$ can be read from the prompt spectrum above the pair creation threshold $\sim \Gamma_{\pm} m_e c^2 \sim$ GeV. Thus, we predict a correlation between the early afterglow and the GeV-TeV prompt emission: a steep decay of X-ray afterglow[9),10)] accompanies a low GeV-TeV energy fraction. Further Fermi-Swift co-observations would be helpful. The shallow X-ray phase[9),10)] could be produced by the (matter-dominated) fast cocoon with $\Gamma \sim 10$–30 that receives energy via photons from $e^{\pm}$-annihilated jets [below Eq. (17)]. The reverse shock emission would be soft because of the increased number of emitting leptons.

• *Cosmic Rays* – The RDISs would produce few ultra high-energy cosmic rays and neutrinos,[50] consistent with the IceCube upper limit.[51] The fast cocoon energized by photons from $e^{\pm}$-annihilated jets might contribute to these emissions.

• *Central engine* – The RDIS model requires less fine tuning of baryon load than previously thought, expanding the parameter space even to the original pure-leptonic model.[3),4)] The baryon load could be prevented by the dipole field near a black hole, which may be rather necessary for the Blandford-Znajek effect to launch a relativistic jet despite nonaxisymmetric turbulence.[52] The ejected Poynting-dominated jet is strongly confined in the star or surrounding matter, possibly dissipating into the radiation-dominated jet via turbulence.

• *Unresolved problems* – We leave the low-energy spectral index[1),2)] $\nu F_{\nu} \propto \nu$ and the Amati and Yonetoku spectral relations[11),12)] for future discussion. Since $\Gamma T' =$ const, the peak energy reflects the initial fireball temperature.

We thank a referee, K. Asano, A. Beloborodov, J. C. McKinney, T. Nakamura

and T. Piran for useful comments. This work is supported by KAKENHI, 19047004, 22244019, 22244030 (KI), 21684014 (KI, YO), 22740131 (NK) and 20105005 (AM).

1) P. Mészáros, Rep. Prog. Phys. **69** (2006), 2259.
2) B. Zhang, Chin. J. Astron. Astrophys. **7** (2007), 1.
3) B. Paczyński, Astrophys. J **308** (1986), L43.
4) J. Goodman, Astrophys. J **308** (1986), L47.
5) A. Shemi and T. Piran, Astrophys. J **365** (1990), L55.
6) M. J. Rees, Mon. Not. R. Astron. Soc. **184** (1978), 61P.
7) M. J. Rees and P. Mészáros, Astrophys. J **430** (1994), L93.
8) S. Kobayashi, T. Piran and R. Sari, Astrophys. J **490** (1997), 92.
9) B. Zhang et al., Astrophys. J **642** (2006), 354.
10) K. Ioka, K. Toma, R. Yamazaki and T. Nakamura, Astron. Astrophys. **458** (2006), 7.
11) L. Amati et al., Astron. Astrophys. **390** (2002), 81.
12) D. Yonetoku et al., Astrophys. J **609** (2004), 935.
13) G. Ghirlanda et al., Astron. Astrophys. **496** (2009), 585.
14) C. Thompson, Mon. Not. R. Astron. Soc. **270** (1994), 480.
15) M. J. Rees and P. Mészáros, Astrophys. J **628** (2005), 847.
16) A. Pe'er and E. Waxman, Astrophys. J. **613** (2004), 448.
17) K. Ioka et al., Astrophys. J **670** (2007), L77.
18) F. Ryde et al., Astrophys. J **709** (2010), L172.
19) K. Ioka, Prog. Theor. Phys. **124** (2010), 667.
20) A. M. Beloborodov, Mon. Not. R. Astron. Soc. **407** (2010), 1033.
21) D. Lazzati and M. C. Begelman, Astrophys. J. **725** (2010), 1137.
22) D. Giannios, Astron. Astrophys. **480** (2008), 305.
23) P. Mészáros and M. J. Rees, Astrophys. J. **530** (2000), 292.
24) A. A. Abdo et al., Science **323** (2009), 1688.
25) M. Ackermann et al., Astrophys. J. **716** (2010), 1178.
26) B. B. Zhang et al., Astrophys. J. **730** (2011), 141.
27) X. Zhao, Z. Li and J. Bai, Astrophys. J. **726** (2011), 89.
28) Y. C. Zou, Y. Z. Fan and T. Piran, Astrophys. J. **726** (2011), L2.
29) R. Hascoet, V. Vennin, F. Daigne and R. Mochkovitch, arXiv:1101.3889.
30) P. Mészáros and M. J. Rees, Astrophys. J. **482** (1997), L29.
31) H. C. Spruit, F. Daigne and G. Drenkhahn, Astron. Astrophys. **369** (2001), 694.
32) S. Komissarov, N. Vlahakis, A. Konigl and M. Barkov, Mon. Not. R. Astron. Soc. **394** (2009), 1182.
33) A. Tchekhovskoy, R. Narayan and J. C. McKinney, New Astron. **15** (2010), 749.
34) M. A. Aloy, E. Mueller, J. M. Ibanez, J. M. Marti and A. MacFadyen, Astrophys. J. **531** (2000), L119.
35) A. Levinson, Int. J. Mod. Phys. A **21** (2006), 6015.
36) O. Bromberg and A. Levinson, Astrophys. J. **671** (2007), 678.
37) M. Shibata, Y. Suwa, K. Kiuchi and K. Ioka, Astrophys. J. **734** (2011), L36.
38) M. C. Begelman and D. F. Cioffi, Astrophys. J. **345** (1989), L21.
39) C. D. Matzner, Mon. Not. R. Astron. Soc. **345** (2003), 575.
40) E. Ramirez-Ruiz, A. Celotti and M. J. Rees, Mon. Not. R. Astron. Soc. **337** (2002), 1349.
41) S. Woosley and A. Heger, Astrophys. J. **637** (2006), 914.
42) A. Mizuta, S. Yamada and H. Takabe, Astrophys. J. **606** (2004), 804.
43) D. Lazzati, B. J. Morsony and M. Begelman, Astrophys. J. **700** (2009), L47.
44) R. Budnik, B. Katz, A. Sagiv and E. Waxman, Astrophys. J. **725** (2010), 63.
45) R. D. Blandford and D. G. Payne, Mon. Not. R. Astron. Soc. **183** (1978), 359.
46) X. Y. Wang, Z. Li, E. Waxman and P. Mészáros, Astrophys. J. **664** (2007), 1026.
47) T. Inoue, K. Asano and K. Ioka, Astrophys. J. **734** (2011), 77.
48) K. Murase and K. Ioka, Astrophys. J. **676** (2008), 1123.
49) K. Toma, X. F. Wu and P. Mészáros, Mon. Not. R. Astron. Soc. **415** (2011), 1663.
50) E. Waxman and J. N. Bahcall, Phys. Rev. Lett. **78** (1997), 2292.
51) R. Abbasi et al. (IceCube Collaboration), Phys. Rev. Lett. **106** (2011), 141101.
52) J. C. McKinney and R. D. Blandford, Mon. Not. R. Astron. Soc. **394** (2009), L126.